COMMUNICATIONS IN NUMERICAL METHODS IN ENGINEERING
Commun. Numer. Meth. Engng 2008; **24**:1019–1032
Published online 5 June 2007 in Wiley InterScience (www.interscience.wiley.com). DOI: 10.1002/cnm.1008

On volumetric locking-free behaviour of *p*-version finite elements under finite deformations

Ulrich Heisserer[1,*,†], Stefan Hartmann[2], Alexander Düster[1] and Zohar Yosibash[3]

[1]*Lehrstuhl für Bauinformatik, Fakultät für Bauingenieur- und Vermessungswesen, Technische Universität München, Munich, Germany*
[2]*Institute of Mechanics, University of Kassel, Kassel, Germany*
[3]*Pearlstone Center for Aeronautical Studies, Department of Mechanical Engineering, Ben-Gurion University of the Negev, Beer-Sheva, Israel*

SUMMARY

We demonstrate the locking-free properties of the displacement formulation of *p*-finite elements when applied to nearly incompressible Neo-Hookean material under finite deformations. For an axisymmetric model problem we provide semi-analytical solutions for a nearly incompressible Neo-Hookean material exploited to investigate the robustness of *p*-FEM with respect to volumetric locking. An analytical solution for the *in*compressible case is also derived to demonstrate the convergence of the compressible numerical solution towards the incompressible case when the compression modulus is increased. Copyright © 2007 John Wiley & Sons, Ltd.

Received 24 July 2006; Revised 26 February 2007; Accepted 22 March 2007

KEY WORDS: *p*-FEM; locking-free; nearly incompressible Neo-Hooke material; finite strains; hyperelasticity; axisymmetry

1. INTRODUCTION

The *p*-version of the finite element method (*p*-FEM) based on the displacement formulation is known to be locking free beyond a moderate polynomial order for nearly incompressible problems in linear elasticity (see [1–3] and references therein). Recently, *p*-FEMs have been shown to be efficient for finite-deformation problems [4, 5], and we demonstrate herein that

*Correspondence to: Ulrich Heisserer, Lehrstuhl für Bauinformatik, Fakultät für Bauingenieur- und Vermessungswesen, Technische Universität München, Arcisstr. 21, 80290 Munich, Germany.
†E-mail: heisserer@bv.tum.de

Contract/grant sponsor: German-Israeli Foundation for Scientific Research and Development; contract/grant number: I-700-26.10/2001

the locking-free property carries over to finite-deformation analyses of nearly incompressible Neo-Hookean materials.

The locking problem has accompanied and fuelled the development of finite elements since the sixties, see for example the synopses of Zienkiewicz and Taylor [6], Hughes [7] and Belytschko *et al.* [8]. Three main strategies to overcome locking can be named: reduced integration with stabilization, mixed methods that either enhance the strain field to compensate for parasitic stresses or eliminate them, and high-order elements. Zienkiewicz and Taylor [9] report that high-order elements are applied with excellent results for incompressible problems [10, 11] but would pose other difficulties and are thus seldom used in practice. In the mean time most difficulties are resolved, see the monographs of Szabó and Babuška [12] and Schwab [13]. For geometrical linear thin Reissner–Mindlin plates it was observed that a moderate polynomial degree of $p=4$ is sufficient to avoid shear locking, see for example Holzer *et al.* [14], Rank *et al*. [15], and Szabó and Babuška [12]. Nübel [16] demonstrates the robustness of geometrical linear p-FEM used in nearly incompressible problems also for the deformation theory of plasticity.

This paper shows that the locking-free properties of p-FEM carry over to geometrical non-linear problems of near incompressibility where hyperelastic constitutive models are used. We investigate the Neo-Hookean model problem of a sphere under internal pressure where a semi-analytical solution exists. This solution is provided in Section 2.1. It serves as a benchmark problem against which p-FEM results are compared to demonstrate that an increase in polynomial order overcomes locking, and to explain amplification of the errors in the stresses for near incompressibility. In Section 4, numerical results demonstrating the locking-free properties of our implementation are provided and discussed for the model problem.

2. CONSTITUTIVE RELATIONS

2.1. A verification example with a semi-analytical solution

In the following, we present a solution for the problem of a sphere under internal pressure (see Figure 1) made of a Neo-Hookean hyperelastic material based on the constitutive assumption

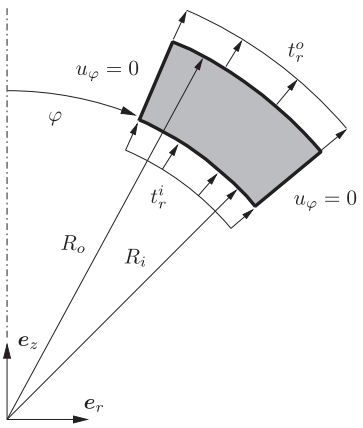

Figure 1. Geometry and dimensions of the sphere of interest ($0 \leqslant \varphi < \pi$, $0 \leqslant \vartheta \leqslant 2\pi$).

DOI: 10.1002/cnm

of compressibility and isotropy. The detailed derivation is provided in [5] so that herein only the main results are summarized.

We denote by capital letters the placement of the material point R, Φ, Θ in the initial configuration, and by lower case letters r, ϕ, ϑ its position in the current configuration where Θ, ϑ denote the circumferential direction. In order to find analytical expressions for a non-trivial case of inhomogeneous deformations (with deformation dependent loads) we consider the following deformation describing a radial inflation of the sphere:

$$r = f(R), \quad \varphi = \Phi, \quad \vartheta = \Theta \quad \text{spherical coordinates} \tag{1}$$

The sphere is considered to be made of a compressible Neo-Hookean material having a strain-energy density function

$$\rho_R \tilde{\psi}(\mathbf{C}) = \frac{K}{2}(J-1)^2 + c_{10}(\mathrm{I}_{\bar{\mathbf{C}}} - 3) \tag{2}$$

$$= \frac{K}{2}(\mathrm{III}_{\mathbf{C}}{}^{1/2} - 1)^2 + c_{10}(\mathrm{I}_{\mathbf{C}}\mathrm{III}_{\mathbf{C}}{}^{-1/3} - 3) \tag{3}$$

$$= \frac{K}{2}(\mathrm{III}_{\mathbf{b}}{}^{1/2} - 1)^2 + c_{10}(\mathrm{I}_{\mathbf{b}}\mathrm{III}_{\mathbf{b}}{}^{-1/3} - 3) = \rho_R \psi(\mathbf{b}) \tag{4}$$

where $\mathbf{C} = \mathbf{F}^{\mathrm{T}}\mathbf{F}$ is the Cauchy–Green tensor and $\mathbf{b} = \mathbf{F}\mathbf{F}^{\mathrm{T}}$ is the left Cauchy–Green tensor, defined in terms of the deformation gradient $\mathbf{F}$. K denotes the compression modulus, J the determinant of the deformation gradient and c_{10} a parameter of the constitutive relation. The first and third invariants of $\mathbf{C}$ (and $\mathbf{b}$) are $\mathrm{I}_{\mathbf{C}} = \mathrm{tr}\,\mathbf{C}$ and $\mathrm{III}_{\mathbf{C}} = \det\mathbf{C}$ (and $\mathrm{I}_{\mathbf{b}} = \mathrm{tr}\,\mathbf{b}$ and $\mathrm{III}_{\mathbf{b}} = \det\mathbf{b}$, respectively). $\mathrm{I}_{\bar{\mathbf{C}}} = \mathrm{I}_{\mathbf{C}}\mathrm{III}_{\mathbf{C}}{}^{-1/3}$ defines the first invariant of the unimodular right Cauchy–Green tensor $\bar{\mathbf{C}} = (\det\mathbf{C})^{-1/3}\mathbf{C}$ resulting from the multiplicative decomposition of the deformation gradient into a volumetric and an isochoric part (see [17] and the literature cited therein).

This specific strain-energy function has been chosen because it describes a compressible deformation becoming increasingly more incompressible as $K \to \infty$. Moreover, it is implemented in many available finite element codes and the solution given here can be used as benchmark example.

The function $f(R)$, if known, determines the deformation and stress state. The radial Cauchy stress, for example, is given by (see [5])

$$\sigma_{rr} = K\left(-1 + \frac{f^2 f'}{R^2}\right) - \frac{4c_{10}(f^2 - f'^2 R^2)}{3\left(\dfrac{f^2 f'}{R^2}\right)^{5/3} R^2} \tag{5}$$

The prime defines the derivative with respect to R, $f' := \mathrm{d}f(R)/\mathrm{d}R$.

Remark 1

The deformation gradient for the inflation of the sphere is $\mathbf{F} = f'\mathbf{e}_r \otimes \mathbf{e}_R + (f/R)\mathbf{e}_\varphi \otimes \mathbf{e}_\Phi + (f/R)\mathbf{e}_\theta \otimes \mathbf{e}_\Theta$, cf. [5, Equation (18)] and its determinant is $\det\mathbf{F} = f^2 f'/R^2$. In the incompressible case the volume must remain constant which is equivalent to the constraint $\det\mathbf{F} = 1$. Hence, the term in (5) in the brackets must vanish. If small errors in the solution f or it's derivative violate this condition, the error is amplified by large $K \gg 1$ for nearly incompressible materials.

DOI: 10.1002/cnm

To determine the function of deformation $f(R)$, the equilibrium equation in r direction, for simplicity without body forces, has to be satisfied (the other two equilibrium equations are identically satisfied for the deformation chosen), leading to the following non-linear second-order ODE:

$$\begin{aligned} & f'' f R \left(20c_{10}f^2 + 4c_{10}f'^2R^2 + 9K\left(\frac{f^2f'}{R^2}\right)^{8/3}R^2\right) \\ & = 22c_{10}f'^4R^3 - 40c_{10}f f'^3R^2 - f'\left(-16c_{10}f^3 - 18fK\left(\frac{f^2f'}{R^2}\right)^{8/3}R^2\right) \\ & \quad - f'^2R\left(-2c_{10}f^2 + 18K\left(\frac{f^2f'}{R^2}\right)^{8/3}R^2\right) \end{aligned} \tag{6}$$

The ODE is supplemented by two boundary conditions: a pressure applied on the inner surface R_i and traction free boundary conditions on the outer surface R_o. These boundary conditions are expressed in terms of (5):

$$\begin{aligned} t_r^\mathrm{i} &= P = K\left(-1 + \frac{f(R_\mathrm{i})^2 f'(R_\mathrm{i})}{R_\mathrm{i}^2}\right) - \frac{4c_{10}\left(f^2(R_\mathrm{i}) - f'^2(R_\mathrm{i})R_\mathrm{i}^2\right)}{3\left(\dfrac{f^2(R_\mathrm{i})f'(R_\mathrm{i})}{R_\mathrm{i}^2}\right)^{5/3}R_\mathrm{i}^2} \\ t_r^\mathrm{o} &= 0 = K\left(-1 + \frac{f(R_\mathrm{o})^2 f'(R_\mathrm{o})}{R_\mathrm{o}^2}\right) - \frac{4c_{10}\left(f^2(R_\mathrm{o}) - f'^2(R_\mathrm{o})R_\mathrm{o}^2\right)}{3\left(\dfrac{f^2(R_\mathrm{o})f'(R_\mathrm{o})}{R_\mathrm{o}^2}\right)^{5/3}R_\mathrm{o}^2} \end{aligned} \tag{7}$$

where P defines the internal pressure.

2.2. Numerical solution

The second-order ODE (6) in combination with the boundary conditions (7) defines a two-point boundary-value problem. It can be solved by a shooting method. In this context, we make use of the algorithm proposed by Engeln-Müllges and Reutter [18] using an explicit fifth-order Runge–Kutta method with an embedded method of fourth order for step-size control. Details are given in [5].

For the subsequent application, solutions for internal pressure $P = 1$ MPa, for a sphere with $R_\mathrm{i} = 10$ mm, $R_\mathrm{o} = 30$ mm, with $c_{10} = \frac{1}{2}$ MPa and increasing bulk modulus $K = 10^k$ MPa, $k = 1, \ldots, 5$ are computed (an accuracy of 10^{-8} is obtained for the displacements). Figure 2 shows the results for $K = 10$ and 100 000. In view of the geometrical linearized theory the material parameters correspond to the shear modulus $\mu = 2c_{10} = 1$ (MPa) or the Poisson ratio $\nu = (3K - 2\mu)/(6K + 2\mu)$, i.e. $\nu = 0.451613$ and 0.499995 for $K = 10$ and 100 000, respectively, see [17]. The solution for those compression moduli sampled at 11 points over the radius is tabulated in Appendix A.

DOI: 10.1002/cnm

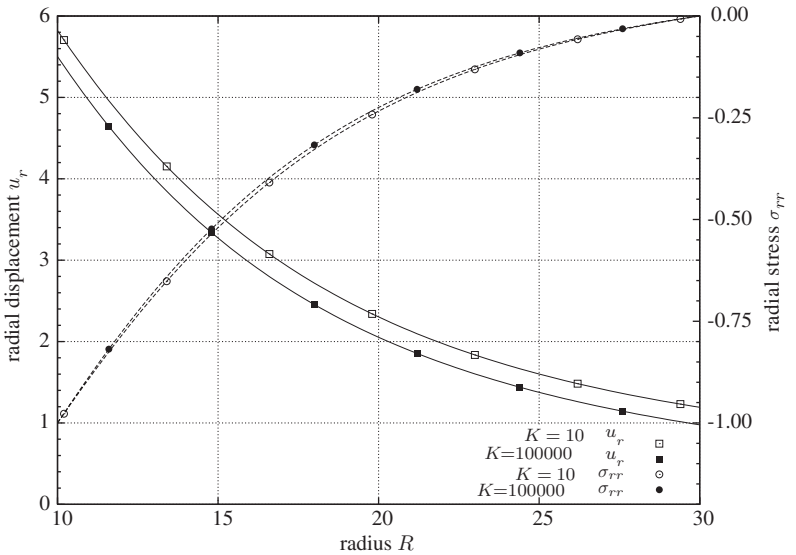

Figure 2. 'Semi-analytical' solution for $K = 10$, 100 000 MPa. $P = 1$ MPa.

3. FINITE ELEMENT DISCRETIZATION

The aforementioned solutions are aimed to serve as benchmark solutions against which numerical results are to be compared to demonstrate the locking-free characteristic and efficiency of p-FEMs applied to finite-deformation nearly incompressible problems. A detailed description of the p-finite element formulation and its application to plane, axisymmetric and 3D domains for geometrically linear and non-linear as well as physically non-linear problems like hyper-elasticity and elastoplasticity can be found in [5, 19]. Since the blending function method is used (see, for example, [12]) the geometry of the discretized domain may be quite complex for 2D and 3D applications. Follower-loads in the context of p-FEM exploiting the blending possibilities are presented in [5]. The overall solution process is realized by applying an incremental/iterative procedure. The non-linear system of equations arising from the spatial discretization based on the p-version is linearized in the light of a Newton–Raphson scheme.

4. NUMERICAL RESULTS

The thick-walled sphere under internal pressure was discretized by two and four p-axisymmetric elements (see meshes in Figure 3) using blending functions for an exact representation of the circular curves. The calculations were done with the academic p-finite element code AdhoC [20]. The main purpose of this example is to demonstrate the convergence characteristics of p-FEMs for progressively more incompressible materials. This is realized by raising the compression modulus $K = 10^k, k = 1, \ldots, 5$. The number of degrees of freedom was increased by uniformly incrementing the polynomial order from 1 to 9 yielding in the two-element case 6, 16, 26, 40, 58, 80, 106, 136

DOI: 10.1002/cnm

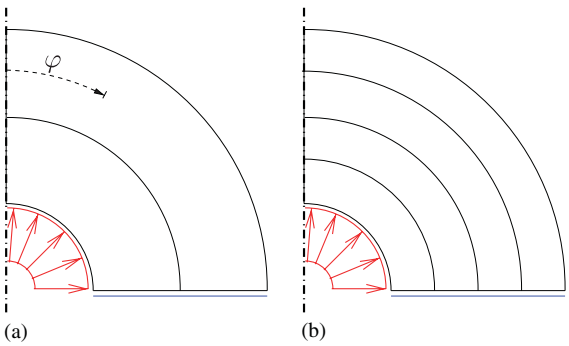

Figure 3. Axisymmetric meshes with curved elements and symmetry boundary condition: (a) two-element p-FE mesh and (b) four-element p-FE mesh.

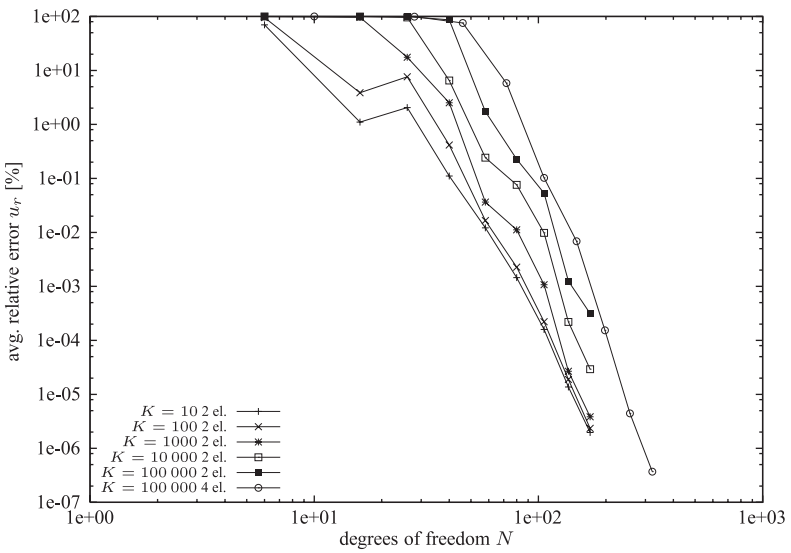

Figure 4. Average relative error in u_r (%).

and 170 degrees of freedom. Throughout all runs 15×15 integration points for each element were used for comparison.

Figure 4 shows the average relative error in displacement u_r in per cent *versus* the degrees of freedom calculated from sampling the data at 101 points along a radial cutline

$$\text{Avg. error} \doteq \frac{1}{101} \sum_{j=1}^{101} \left| \frac{u_r^{\text{EX}}(R_j) - u_r^{\text{FE}}(R_j)}{u_r^{\text{EX}}(R_j)} \right| \times 100 \tag{8}$$

in a log–log scale. As reference the exact solution described in Section 2.2 was evaluated at the sampling points. The average error in radial stress σ_{rr} in per cent calculated in the same manner is shown in Figure 5. Each of the dots corresponds to an increment in the polynomial order of

DOI: 10.1002/cnm

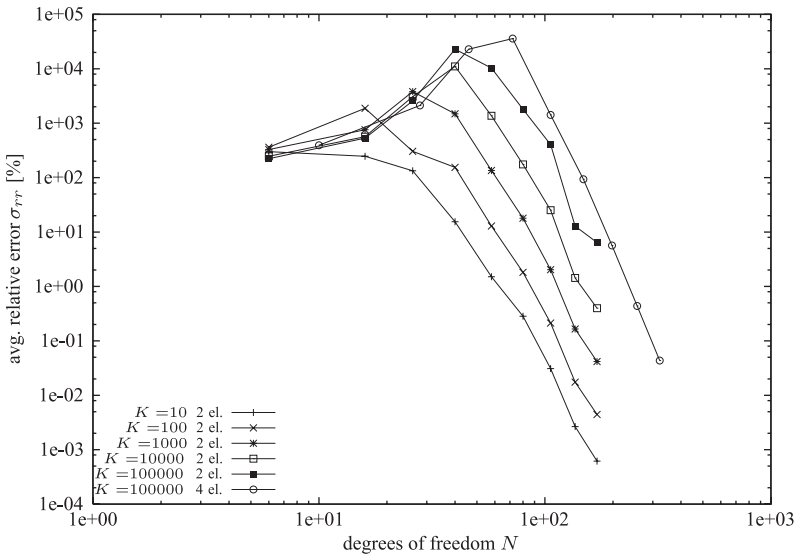

Figure 5. Average relative error in the radial stresses σ_{rr} (%).

one. Hence, it is clearly visible that total locking for the case of two elements and $K = 100\,000$ is present until $p = 4$, afterwards the solution converges rapidly and with $p = 5$ the average error in displacement is already down to less than 2%. If four elements are used $p = 4$ corresponds to an error of about 6% while the error decreases to 0.1% for $p = 5$.

From Figure 5 we can see that the relative error in stress is amplified as the material becomes more and more incompressible. This can be readily explained by noting that in Equation (5) governing the radial stresses any error in the placement $r = f(R)$ or its derivative violating the incompressibility constraint is magnified by K, in our examples K up to 100 000 for the nearly incompressible case. The relative error in stress along a radial cutline in Figure 6 shows that this is not only true in an average sense, but also pointwise.

It is interesting to note that with a moderate number of 170 degrees of freedom ($p = 9$) and only two elements even for the nearly incompressible case of $K = 100\,000$ an average relative error in u_r smaller than 0.000 32% is obtained while the large K results in an average error in σ_{rr} of about 6.5%. However, in the stresses there is rapid convergence for polynomial order $p > 4$ as well. As one would expect from Equation (5) if the bulk modulus is increased by one magnitude also the error in stresses grows approximately one magnitude, this can be verified in Figure 6 and Table AI (compare the values for $p = 9$).

Figure 7 shows how the pointwise deviation from incompressibility ($\det \mathbf{F} = 1$) is decreasing as the compression modulus grows. Using the *in*compressible analytical solution given in Appendix B, we can assess how 'incompressible' is the solution for a given compression modulus K. Note that incompressible solutions are provided for a series of problems for which the internal displacement and pressure are computed that satisfy the equilibrium equations. Figure 8 shows the relative difference in internal pressure in per cent between the (compressible) numerical p-finite element solution and the incompressible reference for a given internal displacement $u_r(R_i)$. For the computations with K up to 10 000 a polynomial order $p = 9$ was sufficient. If the compression

DOI: 10.1002/cnm

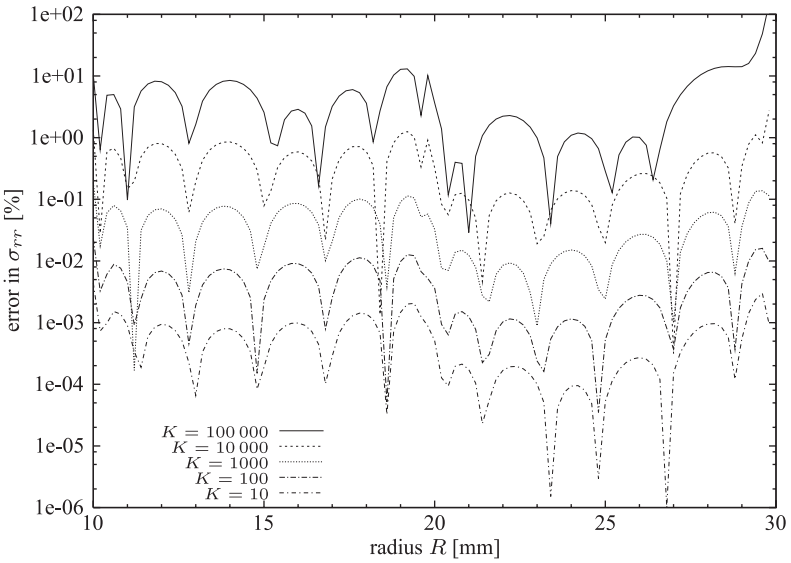

Figure 6. Mesh with two elements, $p = 9$: relative error in σ_{rr} (%) for increasing K.

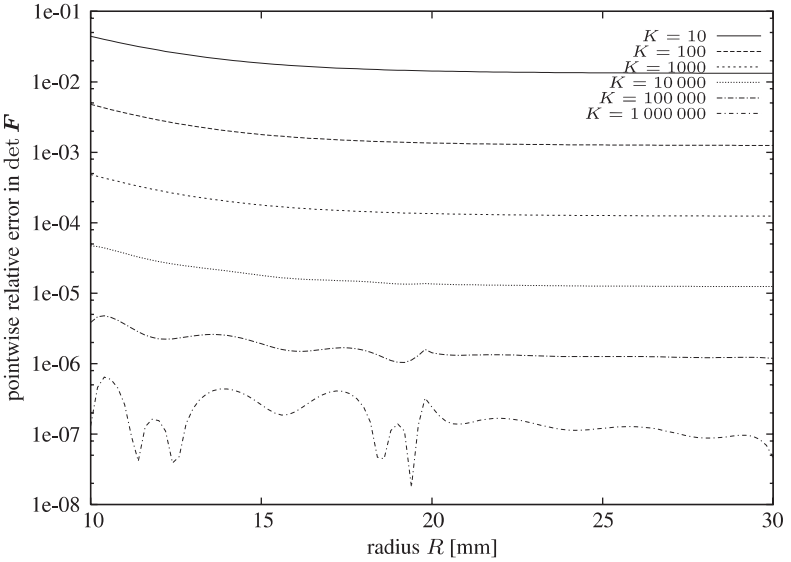

Figure 7. Pointwise error in the incompressibility constraint $|\det \mathbf{F} - 1|$ for $p = 9$.

modulus reaches $K = 100\,000$ the oscillations on a very small scale noticeable in Figure 8(b) vanish if p is raised to 13. In this latter case the plot shows that a relative difference between the compressible semi-analytical solution and the incompressible solution (denoted by the diamond shape) matches the numerical solution.

DOI: 10.1002/cnm

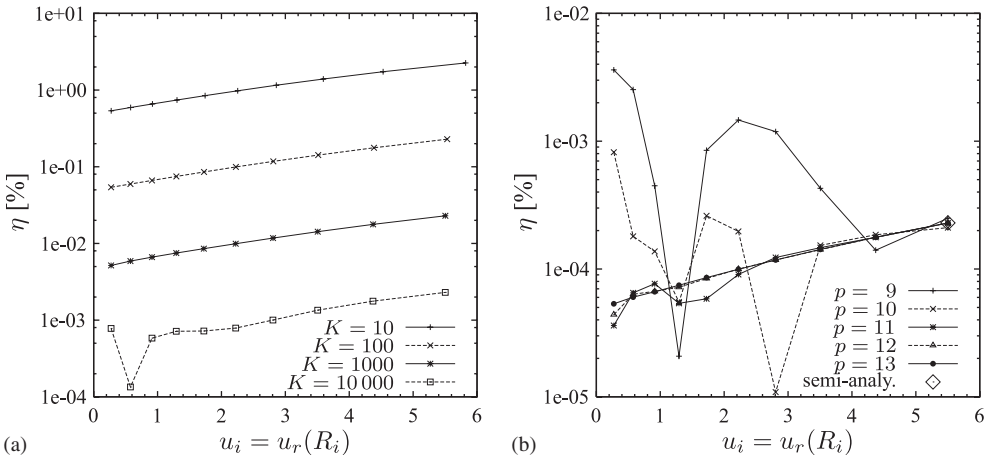

Figure 8. The relative difference $\eta = |P^{\mathrm{FE}}(u_{\mathrm{i}}) - P^{\mathrm{IC}}(u_{\mathrm{i}})/P^{\mathrm{IC}}(u_{\mathrm{i}})| \times 100$ in internal pressure P between the compressible FE solution (two-element mesh) and the incompressible analytic solution as a function of the displacement $u_{\mathrm{i}} = u_r(R_{\mathrm{i}})$. η decreases as K is increased. Note that in (b) the semi-analytic compressible solution for $K = 100\,000$ (computed within an accuracy of 10^{-8} in u_{i}) has an apparently same small relative difference compared to the incompressible result as the FE solution for $p = 13$: (a) $p = 9$, $K = 10 \rightarrow 10\,000$ and (b) $p = 9 \rightarrow 13$, $K = 100\,000$.

Following Suri [3] we can conclude that p-finite elements are locking free in the presented finite-deformation example as the error curves for displacements and stresses in Figures 4 and 5 remain parallel and converge for $p > 4$ also for very high compression moduli K.

5. CONCLUSIONS

We discuss a semi-analytic solution with the compression modulus K as parameter for the finite deformation of a Neo-Hookean sphere under internal pressure. The benchmark solution is used to show that for this model problem the locking-free properties of high-order finite elements well known for geometrically linear problems carry over to the finite-deformation case. The analytical dependence of the stresses on the compression modulus for this model problem readily explains why small errors in the numerically computed displacement are amplified by a large factor K. The example shows that displacement formulations of p finite elements can overcome locking by raising the polynomial order p. Furthermore, the derived analytic solution for the *in*compressible case gives the possibility to assess the relative difference of the compressible solution with a given compression modulus.

APPENDIX A: SOLUTION TABLES

The solution for the investigated compression moduli $K = 10$ to $100\,000$ sampled at 11 points over the radius is tabulated in Tables AI–AIII.

DOI: 10.1002/cnm

Table AI. Sphere under internal pressure: DOF (polynomial order p) and average relative errors in per cent in u_r and σ_{rr} for p-FE solutions.

DOF (p) two elements	Average error (u_r) % $K = 10$	Average error (u_r) % $K = 100$	Average error (u_r) % $K = 1000$	Average error (u_r) % $K = 10\,000$	Average error (u_r) % $K = 100\,000$
6 (1)	6.983280846E+01	9.5269932E+01	9.907157826E+01	9.981561118E+01	9.997844902E+01
16 (2)	1.101921483E+00	3.8662678E+00	9.646173999E+01	9.942663224E+01	9.986553204E+01
26 (3)	2.055641371E+00	7.6180657E+00	1.756328147E+01	9.595459426E+01	9.974518752E+01
40 (4)	1.108291789E−01	4.1478166E−01	2.521988004E+00	6.506828996E+00	8.661859778E+01
58 (5)	1.212597316E−02	1.6560222E−02	3.635192519E−02	2.417838390E−01	1.727937377E+00
80 (6)	1.452696466E−03	2.2684369E−03	1.115035145E−02	7.609565235E−02	2.270126864E−01
106 (7)	1.595114879E−04	2.2172175E−04	1.075499406E−03	9.814558987E−03	5.323631678E−02
136 (8)	1.370535820E−05	1.8897797E−05	2.677895669E−05	2.198140702E−04	1.251180778E−03
170 (9)	1.964790025E−06	2.3470184E−06	3.853879283E−06	2.920482985E−05	3.145745740E−04
DOF (p) two elements	Average error (σ_{rr}) % $K = 10$	Average error (σ_{rr}) % $K = 100$	Average error (σ_{rr}) % $K = 1000$	Average error (σ_{rr}) % $K = 10\,000$	Average error (σ_{rr}) % $K = 100\,000$
6 (1)	3.006689337E+02	3.6220284E+02	3.276664797E+02	2.462204001E+02	2.229869114E+02
16 (2)	2.465804728E+02	1.8789976E+03	7.591388343E+02	5.637689561E+02	5.328481905E+02
26 (3)	1.337053119E+02	3.0415066E+02	3.804915473E+03	3.068254348E+03	2.564841507E+03
40 (4)	1.547535621E+01	1.5451258E+02	1.487362855E+03	1.105656722E+04	2.290003269E+04
58 (5)	1.511532528E+00	1.2900826E+01	1.353470545E+02	1.367770978E+03	1.029684008E+04
80 (6)	2.842779005E−01	1.8132423E+00	1.795774934E+01	1.748979049E+02	1.803357358E+03
106 (7)	3.098556237E−02	2.1263489E−01	2.031664676E+00	2.526832023E+01	4.039467240E+02
136 (8)	2.658960948E−03	1.7439388E−02	1.657037181E−01	1.433039045E+00	1.284992373E+01
170 (9)	6.173770274E−04	4.4520136E−03	4.174696015E−02	3.993825467E−01	6.420052203E+00

DOI: 10.1002/cnm

Table AII. Semi-analytical solution (cf. Section 2.2) with an accuracy in displacements of 10^{-8} for internal pressure P=1 MPa, R_i=10 mm, $R_\mathrm{o} = 30$ mm, $c_{10} = \frac{1}{2}$ MPa and increasing bulk modulus $K = 10, 100, 1000$ MPa.

R	$r = f(R)$	$u_r(R) = r - R$	$f'(R)$	$\sigma_{rr}(R)$	$\sigma_{\vartheta\vartheta}(R)$
$K = 10$					
10.0	1.58207959544736E+01	5.82079595447360E+00	4.17267721341883E−01	−1.00000000000000E+00	1.16616541958393E+00
12.0	1.67663669768742E+01	4.76636697687430E+00	5.26670833886427E−01	−7.84585042800661E−01	8.14479732782215E−01
14.0	1.79186472372307E+01	3.91864723723080E+00	6.22997029487430E−01	−5.99911097091279E−01	6.08419042480270E−01
16.0	1.92472244700820E+01	3.24722447008210E+00	7.02755681346734E−01	−4.48403248016017E−01	4.78487517669625E−01
18.0	2.07187718241106E+01	2.71877182411070E+00	7.66229259875702E−01	−3.27897982220234E−01	3.91602849170722E−01
20.0	2.23027542264333E+01	2.30275422643340E+00	8.15636697716700E−01	−2.33810734588993E−01	3.30961786633944E−01
22.0	2.39737802730011E+01	1.97378027300120E+00	8.53728231214495E−01	−1.60971051718994E−01	2.87311695700626E−01
24.0	2.57118366341894E+01	1.71183663418950E+00	8.83058084049778E−01	−1.04653794499719E−01	2.55150148313772E−01
26.0	2.75015842508475E+01	1.50158425084760E+00	9.05729415519818E−01	−6.09611479894031E−02	2.31001115476809E−01
28.0	2.93314127197658E+01	1.33141271976590E+00	9.23374951886491E−01	−2.68475632479659E−02	2.12571907331587E−01
30.0	3.11925612965790E+01	1.19256129657910E+00	9.37225904967904E−01	3.28931760301687E−14	1.98303331177820E−01
$K = 100$					
10.0	1.55323930872015E+01	5.53239308720150E+00	4.16491846011322E−01	−1.00000000000002E+00	1.22125728715591E+00
12.0	1.64825963084550E+01	4.48259630845510E+00	5.31564170403188E−01	−7.77333979437615E−01	8.19101879943810E−01
14.0	1.76478159682778E+01	3.64781596827790E+00	6.30595890142312E−01	−5.89428658828810E−01	5.97924461347605E−01
16.0	1.89923866758160E+01	2.99238667581610E+00	7.10869697716100E−01	−4.37407917492169E−01	4.63826800884639E−01
18.0	2.04795824711094E+01	2.47958247110950E+00	7.73627184793020E−01	−3.17956072070976E−01	3.76352639849649E−01
20.0	2.20771643211538E+01	2.07716432115390E+00	8.21792444353112E−01	−2.25636868576499E−01	3.16297469527876E−01
22.0	2.37591389362172E+01	1.75913893621730E+00	8.58522371534378E−01	−1.54755611933291E−01	2.73565100679880E−01
24.0	2.55054769395087E+01	1.50547693950880E+00	8.86567216154800E−01	−1.00313812693260E−01	2.42343970039143E−01
26.0	2.73010822042729E+01	1.30108220427300E+00	9.08105783424110E−01	−5.82968078970362E−02	2.19049040132768E−01
28.0	2.91346708587921E+01	1.13467085879220E+00	9.24786282019107E−01	−2.56270317014439E−02	2.01357693124189E−01
30.0	3.09978092767006E+01	9.97809276700700E−01	9.37828978135077E−01	2.00323590181239E−13	1.87712002254115E−01
$K = 1000$					
10.0	1.55049853575450E+01	5.50498535754500E+00	4.16167640080821E−01	−1.00000000000015E+00	1.22904427668645E+00
12.0	1.64553264672247E+01	4.45532646722480E+00	5.31954508913815E−01	−7.76556212882675E−01	8.20103202427150E−01
14.0	1.76217119346290E+01	3.62171193462910E+00	6.31317103810022E−01	−5.88324141604895E−01	5.97025512751605E−01
16.0	1.89678305666577E+01	2.96783056665780E+00	7.11664598079222E−01	−4.36264096805939E−01	4.62410613149170E−01
18.0	2.04565675676679E+01	2.45656756766800E+00	7.74358599082473E−01	−3.16931715432072E−01	3.74848359355015E−01
20.0	2.20554967321618E+01	2.05549673216190E+00	8.22403431372430E−01	−2.24800802862645E−01	3.14842742774102E−01
22.0	2.37385598160292E+01	1.73855981602930E+00	8.58999915807093E−01	−1.54123399131127E−01	2.72199219971642E−01
24.0	2.54857247622825E+01	1.48572476228260E+00	8.86918761232835E−01	−9.98742510940274E−02	2.41071100319598E−01
26.0	2.72819194751374E+01	1.28191947513750E+00	9.08346451409759E−01	−5.80278499762930E−02	2.17861115468411E−01
28.0	2.91158924863800E+01	1.11589248638010E+00	9.24932690953111E−01	−2.55041395090912E−02	2.00243239185618E−01
30.0	3.09792425145777E+01	9.79242514577798E−01	9.37896598194558E−01	−6.61667519819692E−12	1.86659552803081E−01

Commun. Numer. Meth. Engng 2008; **24**:1019–1032
DOI: 10.1002/cnm

Table AIII. Semi-analytical solution (cf. Section 2.2) with an accuracy in displacements of 10^{-8} for internal pressure $P = 1\,\text{MPa}$, $R_\text{i} = 10\,\text{mm}$, $R_\text{o} = 30\,\text{mm}$, $c_{10} = \frac{1}{2}\,\text{MPa}$ and increasing bulk modulus $K = 10\,000$, $100\,000\,\text{MPa}$.

R	$r = f(R)$	$u_r(R) = r - R$	$f'(R)$	$\sigma_{rr}(R)$	$\sigma_{\vartheta\vartheta}(R)$
$K = 10\,000$					
10.0	1.55022561638923E+01	5.50225616389230E+00	4.16132190763150E−01	−9.99999999999363E−01	1.22985262927624E+00
12.0	1.64526073286286E+01	4.45260732862870E+00	5.31992529226571E−01	−7.76477693338393E−01	8.20209396170670E−01
14.0	1.76191082383409E+01	3.61910823834100E+00	6.31388971847781E−01	−5.88212869782237E−01	5.96936928223621E−01
16.0	1.89653814614825E+01	2.96538146148260E+00	7.11744091783385E−01	−4.36149032139154E−01	4.62269181099325E−01
18.0	2.04542726828889E+01	2.45427268288900E+00	7.74431820731630E−01	−3.16828776940395E−01	3.74697833014070E−01
20.0	2.20533367643711E+01	2.05333676437120E+00	8.22464631082691E−01	−2.24716851814078E−01	3.14697107710820E−01
22.0	2.37365089053511E+01	1.73650890535120E+00	8.59047778749094E−01	−1.54059954902603E−01	2.72062466456985E−01
24.0	2.54837567691768E+01	1.48375676917690E+00	8.86954030654035E−01	−9.98301597430556E−02	2.40943660003763E−01
26.0	2.72800106640754E+01	1.28001066407550E+00	9.08370640735113E−01	−5.80008807583124E−02	2.17742183374997E−01
28.0	2.91140223644655E+01	1.11402236446560E+00	9.24947462883162E−01	−2.54918200026978E−02	2.00131665909748E−01
30.0	3.09773938244832E+01	9.77393824483300E−01	9.37903499933854E−01	6.13744072382703E−11	1.86554189202265E−01
$K = 100\,000$					
10.0	1.55019833590061E+01	5.50198335900610E+00	4.16128614693349E−01	−9.99999999985062E−01	1.22993377104841E+00
12.0	1.64523354910917E+01	4.45233549109180E+00	5.31996320999158E−01	−7.76469833661090E−01	8.20220077422705E−01
14.0	1.76188479336418E+01	3.61884793364190E+00	6.31396156190941E−01	−5.88201734170152E−01	5.96928082871814E−01
16.0	1.89651366140862E+01	2.96513661408630E+00	7.11752041310214E−01	−4.36137518870117E−01	4.62255039344947E−01
18.0	2.04540432587759E+01	2.45404325877600E+00	7.74391438220739E−01	−3.16818478197511E−01	3.74682778886406E−01
20.0	2.20531208340464E+01	2.05312083404650E+00	8.22470752174731E−01	−2.24708453324768E−01	3.14682542193657E−01
22.0	2.37363038830478E+01	1.73630388304790E+00	8.59052566225307E−01	−1.54053608203183E−01	2.72048789222553E−01
24.0	2.54835600410434E+01	1.48356004104350E+00	8.86957558828580E−01	−9.98257492538874E−02	2.40930914209705E−01
26.0	2.72798198566730E+01	1.27981985667310E+00	9.08373606964216E−01	−5.79981830587238E−02	2.17730288619287E−01
28.0	2.91138354286447E+01	1.11383542864480E+00	9.24948941447635E−01	−2.54905876630848E−02	2.00120507226798E−01
30.0	3.09772090346658E+01	9.77209034665901E−01	9.37904191557690E−01	2.01086201238442E−10	1.86543651650604E−01

DOI: 10.1002/cnm

APPENDIX B: ANALYTICAL SOLUTION FOR THE SPHERE UNDER INTERNAL PRESSURE

In the case of the Neo-Hookean elasticity under the assumption of (isotropy and) incompressibility it is possible to derive an analytical solution for the boundary-value problem of a thick-walled sphere under internal pressure. Let the deformation be described in spherical coordinates. Then, the deformation has the form: $r = f(R)$, $\varphi = \Phi$, $\vartheta = \Theta$. The deformation gradient $\mathbf{F} = \mathrm{Grad}\,\boldsymbol{\varphi}(\mathbf{X}, t) = \partial\varphi^k(X^1, X^2, X^3, t)/\partial X^K \mathbf{g}_i \otimes \mathbf{G}^K$ reads

$$\mathbf{F} = \begin{bmatrix} f'(R) & 0 & 0 \\ 0 & f(R)/R & 0 \\ 0 & 0 & f(R)/R \end{bmatrix} \mathbf{e}_k \otimes \mathbf{e}_l, \quad k, l = r, \varphi, \vartheta \tag{B1}$$

with the tangent vectors $\mathbf{g}_1 = \mathbf{e}_r$, $\mathbf{g}_2 = r\mathbf{e}_\varphi$, and $\mathbf{g}_3 = r\sin\varphi\mathbf{e}_\vartheta$, as well as the gradient vectors $\mathbf{G}^1 = \mathbf{e}_r$, $\mathbf{G}^2 = (1/R)\mathbf{e}_\varphi$, and $\mathbf{G}^3 = (R\sin\Phi)^{-1}\mathbf{e}_\vartheta$. In the case of incompressibility, $\det\mathbf{F} = 1$ must hold leading to the ODE $f'(R)f^2(R)/R^2 = 1$, with the result $f(R) = (R^3 + B)^{1/3}$. B defines an undetermined integration constant defined later on by the stress boundary condition. The left Cauchy–Green tensor $\mathbf{b} = \mathbf{F}\mathbf{F}^{\mathrm{T}}$ reads $\mathbf{b} = \mathrm{diag}(f'^2, (f/R)^2, (f/R)^2)$ relative to the basis $\mathbf{e}_r$, $\mathbf{e}_\varphi$, $\mathbf{e}_\vartheta$. The Neo-Hookean material is defined by $\boldsymbol{\sigma} = -\tilde{p}\mathbf{I} + 2c_{10}\mathbf{b}$, $\boldsymbol{\sigma}$ symbolizes the Cauchy stress tensor, i.e. in coordinate representation

$$\sigma_{rr} = -\tilde{p} + 2c_{10}(R/r)^4, \quad \sigma_{\varphi\varphi} = \sigma_{\vartheta\vartheta} = -\tilde{p} + 2c_{10}(r/R)^2 \tag{B2}$$

$\tilde{p}$ is the undetermined pressure of the reaction stress guaranteeing the constraint $\det\mathbf{F} = 1$. The equilibrium condition

$$\frac{\partial\sigma_{rr}}{\partial r} + 2\frac{\sigma_{rr} - \sigma_{\vartheta\vartheta}}{r} = 0 \tag{B3}$$

defines an ODE

$$\sigma'_{rr}(r) = 4c_{10}(r^6 - R^6)/(r^5R^2) \tag{B4}$$

having the solution

$$\sigma_{rr}(r) = -P + c_{10}\left(\frac{(r^3 - B)^{1/3}(5r^3 - B)}{r^4} - \frac{(r_i^3 - B)^{1/3}(5r_i^3 - B)}{r_i^4}\right) \tag{B5}$$

where the boundary condition $\sigma_{rr}(r_i) = -P$ and the relation $R = (r^3 - B)^{1/3}$ are exploited. P is again the internal pressure. From Equation (B5) the integration constant B can be determined if a stress-free outer surface is assumed, $\sigma_{rr}(r_o) = 0$,

$$P = c_{10}\left(\frac{R_o(5R_o^3 + 4B)}{(R_o^3 + B)^{4/3}} - \frac{R_i(5R_i^3 + 4B)}{(R_i^3 + B)^{4/3}}\right) \tag{B6}$$

R_o is the outer radius and R_i the inner radius in the initial configuration. For $u_i = r_i - R_i = (R_i^3 + B)^{1/3} - R_i$ it becomes obvious that $B = (u_i + R_i)^3 - R_i^3$ corresponds to the displacement u_i at the inner radius. This implies that for given u_i the internal pressure P can be computed by function evaluation of Equation (B6), or, *vice versa*, for given P, B must be computed iteratively.

DOI: 10.1002/cnm

ACKNOWLEDGEMENTS

The authors gratefully acknowledge the support of this work by the German-Israeli Foundation for Scientific Research and Development under grant number I-700-26.10/2001.

REFERENCES

1. Babuška I, Suri M. Locking effects in the finite element approximation of elasticity problems. *Numerische Mathematik* 1992; **62**:439–463.
2. Babuška I, Suri M. On locking and robustness in the finite element method. *SIAM Journal on Numerical Analysis* 1992; **29**:1261–1293.
3. Suri M. Analytical and computational assessment of locking in the *hp* finite element method. *Computer Methods in Applied Mechanics and Engineering* 1996; **133**:347–371.
4. Düster A, Hartmann S, Rank E. *p*-FEM applied to finite isotropic hyperelastic bodies. *Computer Methods in Applied Mechanics and Engineering* 2003; **192**:5147–5166.
5. Yosibash Z, Hartmann S, Heisserer U, Düster A, Rank E, Szanto M. Axisymmetric pressure boundary loading for finite deformation analysis using *p*-FEM. *Computer Methods in Applied Mechanics and Engineering* 2007; **196**(7):1261–1277.
6. Zienkiewicz OC, Taylor RL. *The Finite Element Method—Solid Mechanics*, vol. 2 (5th edn). Butterworth-Heinemann: London, 2000.
7. Hughes TJR. *The Finite Element Method*. Dover: New York, 2000.
8. Belytschko T, Liu WK, Moran B. *Nonlinear Finite Elements for Continua and Structures*. Wiley: New York, 2000.
9. Zienkiewicz OC, Taylor RL. *The Finite Element Method—The Basis*, vol. 1 (5th edn). Butterworth-Heinemann: London, 2000.
10. Arnold DN. Discretization by finite elements of a model parameter dependent problem. *Numerische Mathematik* 1981; **37**:405–421.
11. Vogelius M. An analysis of the *p*-version of the finite element method for nearly incompressible materials; uniformly optimal error estimates. *Numerische Mathematik* 1983; **41**:39–53.
12. Szabó BA, Babuška I. *Finite Element Analysis*. Wiley: New York, 1991.
13. Schwab Ch. *p- and hp-Finite Element Methods*, *Theory and Applications in Solid and Fluid Mechanics*. Oxford University Press: Oxford, 1998.
14. Holzer S, Rank E, Werner H. An implementation of the *hp*-version of the finite element method for Reissner–Mindlin plate problems. *International Journal for Numerical Methods in Engineering* 1990; **30**:459–471.
15. Rank E, Krause R, Preusch K. On the accuracy of *p*-version elements for the Reissner–Mindlin plate problem. *International Journal for Numerical Methods in Engineering* 1998; **43**:51–67.
16. Nübel V. Die adaptive *rp*-Methode für elastoplastische Probleme. *Ph.D. Thesis*, Lehrstuhl für Bauinformatik, Technische Universität München, 2005.
17. Hartmann S, Neff P. Polyconvexity of generalized polynomial-type hyperelastic strain energy functions for near-incompressibility. *International Journal of Solids and Structures* 2003; **40**(11):2767–2791.
18. Engeln-Müllges G, Reutter F. *Formelsammlung zur Numerischen Mathematik mit Standard-FORTRAN 77-Programmen*. B.I. Wissenschaftsverlag, Mannheim, 1986.
19. Düster A. High order finite elements for three-dimensional, thin-walled nonlinear continua. *Ph.D. Thesis*, Lehrstuhl für Bauinformatik, Fakultät für Bauingenieur- und Vermessungswesen, Technische Universität München (Available from: http://www.inf.bv.tum.de/~duester) 2001.
20. Düster A, Bröker H, Heidkamp H, Heißerer U, Kollmannsberger S, Krause R, Muthler A, Niggl A, Nübel V, Rücker M, Scholz D. *AdhoC*^{4}*—User's Guide*. Lehrstuhl für Bauinformatik, Technische Universität München, 2004.

DOI: 10.1002/cnm